Published in final edited form as:

*Int J Hyperthermia*. 2012 ; 28(4): 337–348. doi:10.3109/02656736.2012.677930.

# Targeted drug delivery by high intensity focused ultrasound mediated hyperthermia combined with temperature-sensitive liposomes: Computational modelling and preliminary *in vivo* validation

**Astrid Gasselhuber**[1], **Matthew R. Dreher**[2], **Ari Partanen**[2,3,4], **Pavel S. Yarmolenko**[2,5], **David Woods**[2], **Bradford J. Wood**[2], **Dieter Haemmerich**[1,6]

[1]Department of Pediatrics, Medical University of South Carolina, Charleston, South Carolina, USA [2]Center for Interventional Oncology, Clinical Center, National Cancer Institute, National Institutes of Health, Bethesda, Maryland, USA [3]Department of Physics, University of Helsinki, Helsinki, Finland [4]Philips Healthcare, Cleveland, Ohio, USA [5]Department of Biomedical Engineering, Duke University, Durham, North Carolina, USA [6]Department of Bioengineering, Clemson University, Clemson, South Carolina, USA

## Abstract

**Purpose—**To develop and validate a computational model that simulates 1) tissue heating with high intensity focused ultrasound (HIFU), and 2) resulting hyperthermia-mediated drug delivery from temperature-sensitive liposomes (TSL).

**Materials and methods—**HIFU heating in tissue was simulated using a heat transfer model based on the bioheat equation, including heat-induced cessation of perfusion. A spatio-temporal multi-compartment pharmacokinetic model simulated intravascular release of doxorubicin from TSL, its transport into interstitium, and cell uptake. Two heating schedules were simulated, each lasting 30 min: 1) hyperthermia at 43°C (HT) and 2) hyperthermia followed by a high temperature (50°C for 20 s) pulse (HT+). As preliminary model validation, *in vivo* studies were performed in thigh muscle of a New Zealand White rabbit, where local hyperthermia with a clinical magnetic resonance-guided HIFU system was applied following TSL administration.

**Results—**HT produced a defined region of high doxorubicin concentration (cellular concentration ~15–23 μg/g) in the target region. Cellular drug uptake was directly related to HT duration, with increasing doxorubicin uptake up to ~2 h. HT+ enhanced drug delivery by ~40% compared to HT alone. Temperature difference between model and experiment within the hyperthermia zone was on average 0.54°C. Doxorubicin concentration profile agreed qualitatively with *in vivo* fluorescence profile.

Correspondence: Dieter Haemmerich, Department of Pediatrics, Medical University of South Carolina, 165 Ashley Ave, MSC 915 Charleston, SC 29425, South Carolina, USA. Tel: 843-792-1396. Fax: 843-792-5878. haemmerich@ieee.org.

***Declaration of Interest:***

The other authors report no conflicts of interest. The authors alone are responsible for the content and writing of the paper.

**Conclusions—**Computational models can predict temperature and delivered drug from combination of HIFU with TSL. Drug delivery using TSL may be enhanced by prolonged hyperthermia up to 2 h or by local cessation of vascular perfusion with a high temperature pulse following hyperthermia.

### Keywords

drug delivery; focused ultrasound; hyperthermia; liposome; MR-HIFU; TSL

## Introduction

Current chemotherapy regimens in clinical use are limited by severe systemic toxicity. To reduce dose-limiting toxicity and improve tumour drug delivery, numerous drug delivery systems (DDS) have been developed. Liposomes are one of the few DDS that are in clinical use [1], and can target the tumour both passively and actively. Passive tumour targeting of liposomes involves their accumulation in tumour tissue through leaky tumour vasculature via enhanced permeability and retention (EPR) effect [2]. Active targeting of a tumour with liposomes can be achieved through various means, one of them being triggered intravascular release. An example of such targeting via triggered release is the use of temperature-sensitive liposomal carriers, which have gained considerable attention and have been used in several clinical trials [3–7].

Temperature-sensitive liposomes (TSL) are DDS that release content (usually a chemotherapy agent) above a threshold temperature, typically ~40°C [8–13]. Mild hyperthermia (40–45°C) in conjunction with liposomes can increase passive liposome tumour accumulation [14], likely by enhancing the EPR effect. However, accumulation due to EPR requires considerably more time than is afforded by the relatively fast clearance of TSL [11]. Therefore, most tumour-specific drug delivery through the combination of mild hyperthermia and TSL is likely due to heat-triggered intravascular release [14]. Fast-releasing TSL (i.e. release within several seconds) [15–17] are well suited for intra-vascular triggered release, as they can release their contents within the typically few seconds lasting transit time of the tumour vascular network [18–20].

Localised hyperthermia as required for triggering drug release from TSL can be achieved by a variety of methods including radiofrequency electric current, microwaves, laser, as well as high intensity focused ultrasound (HIFU). Of these heating methods, HIFU is superior in terms of controlled, noninvasive heating of precisely targeted tissues [21–24]. Several recent studies demonstrated that the combination of TSL with HIFU allows for non-invasive targeting of drug delivery [25–29].

A variety of physiological, biological, biophysical, DDS, and drug parameters affect hyperthermia-mediated drug delivery from TSL. Computer simulations provide a means to efficiently examine effects of these parameters. Among other benefits offered by computer simulations, they can suggest optimal delivery strategies by enabling detailed examination of heating algorithms (e.g. varying temperature and time), varying tumour transport parameters (e.g. vessel permeability, perfusion), and modifying TSL properties (e.g. release rate). *In silico* models have provided accurate descriptions of thermal therapies and drug delivery via

TSL and other carriers [30–32, 16, 28]. Here, we present a mathematical model that combines a heat transfer model with a drug delivery model to simulate both HIFU-induced tissue heating and hyperthermia-mediated drug delivery from TSL-encapsulated doxorubicin (TSL-DOX). The model includes heat-induced changes in perfusion – which in turn affect drug delivery. This feature of the model allowed examination of a novel strategy: a brief temperature elevation above the mild hyperthermia range was used following heat-induced delivery to cause local vascular shutdown, forming a drug depot. Further, the effect of hyperthermia duration on delivered drug was examined, and the results of simulations were compared to an *in vivo* study.

## Methods

To simulate HIFU-induced tissue heating and resulting drug delivery of DOX delivered via TSL, we combined two spatiotemporal finite element models: 1) a heat transfer model based on the bioheat equation, and 2) a drug delivery model [16, 28]. The two models were coupled in that temperature and perfusion were fed from the heat transfer into the drug delivery model. The current model extends upon prior models by estimating the cancer cell survival fraction due to both thermal exposure as well as DOX uptake. The finite element software Comsol (Version 3.5 a) was used for both the heat transfer and the drug delivery model. The models were implemented as 2D axially symmetric. Temporal resolution was 0.3–2 s, and triangular element size was 0.5–2.5 mm.

### Simulation of HIFU heating

The heat transfer model used the bioheat equation [33] to simulate tissue heating (Equation 1), with parameters listed in Table 1.

$$\rho c\frac{\partial T}{\partial t} = \nabla \cdot (k\nabla T) + k_{HIFU} \cdot Q_{HIFU} - DP \cdot \rho_{bl} c_{bl} w_{bl}(T - T_{bl}) \quad (1)$$

In this equation, $DP$ refers to the decrease in perfusion due to heat-induced coagulation, where $DP$ is 1 initially and becomes 0 at complete vascular shutdown. The HIFU heat source term (power density profile $Q_{HIFU}$ (W/m$^3$)) was calculated based on MR thermometry data from a phantom study as follows:

Sonications with a clinical MR-HIFU system (Sonalleve 1.5 T, Philips Medical Systems, Vantaa, Finland) were performed in a tissue-mimicking agar-silica gel phantom (2 wt% agar and 2 wt% silica particles) [34]. An 8-mm diameter target region was sonicated for 30 s at 100 W power, and 1.2 MHz frequency. Temperature was monitored in slices both perpendicular and parallel to the beam axis centred at the target region. Temperature was monitored by a multishot RF-spoiled FFE-EPI sequence with 7 k-space lines acquired per excitation. Imaging parameters were: TR = 54 ms, TE = 30 ms, matrix of 144 × 144, FOV of 200 × 200 mm$^2$, slice thickness of 7 mm, flip angle = 19°, bandwidth=252 Hz, and a 121-binomial water-selective excitation pulse. The spatial resolution was 1.39 mm × 1.39 mm × 7.0 mm, with temporal sampling time of 2.5 s. Temperature maps were calculated in real time via proton resonance frequency shift (PRFS) technique [35]. Temperature maps were

corrected for baseline drift by referencing temperature change to a reference region in proximity, but outside the heated region.

Initial rate of temperature rise for each voxel (bilinear approximation of the first 10 s of heating) was calculated, from which the HIFU heat source term $Q_{HIFU}$ in Equation 1 was determined.

To maintain a constant temperature throughout the simulation, a proportional-integral (PI) controller was implemented that adjusted applied power using temperature $T$ at the centre of the heated region as control temperature location:

$$k_{HIFU} = k_p(T_{set} - T) + k_i \int T_{set} - T \tag{2}$$

To model decrease of perfusion ($DP$) due to vascular coagulation, an Arrhenius model was used:

$$DP = \exp - \left( \int_0^t A e^{-\Delta E/[RT(\tau)]} \mathrm{d}\tau \right) \tag{3}$$

Arrhenius parameters $A$ (frequency factor) and $\Delta E$ (activation energy) were determined by fitting Equation 3 to experimental data from a prior study [36]. To calculate the expected cell survival fraction ($ESF$) due to thermal damage; also an Arrhenius damage model was used (i.e. the same as Equation 3, substituting $ESF$ for $DP$, and with different parameters $A$, $\Delta E$) based on Arrhenius parameters from a prior study [37].

## Simulation of TSL drug delivery

An overview of the drug delivery model is presented in Figure 1. The tumour was represented by three compartments: 1) plasma, 2) extracellular-extravascular space (EES), and 3) intracellular space. These compartments were considered spatially varying, i.e. each location within the tumour was associated with individual drug concentrations for each compartment. In addition, a lump tissue body compartment (representing all body tissues except tumour), and a lump plasma compartment were considered (not shown in Figure 1). Pharmacokinetics of DOX after release were based on prior studies [40], and a published DOX cell uptake model based on *in vitro* studies in a lung cancer cell line was implemented, where both active and passive transport mechanisms are considered [41].

TSL-DOX was administered as a bolus injection at a dose of 1.21 mg/kg body weight (corresponding to a total dose of 85 mg in a 70 kg human), considering pharmacokinetic data of this TSL formulation [7] in the model. Spatially and temporally varying temperature and perfusion calculated by the heat transfer model were used as input data in the drug delivery model. Local temperature dictated the rate of release of DOX from TSL in plasma. Temperature-dependent release rate was implemented based on prior *in vitro* measurements (e.g. complete release in ~5 s at 40°C) [16]. Following release in plasma, DOX crosses the vessel wall into the EES, and is taken up by cells.

The drug delivery model consists of ordinary differential equations (ODEs), one for each compartment. All concentrations refer to free DOX, except $c_{p\_TSL}$, which describes TSL-DOX concentration. Subscripts for concentrations refer to various compartments (p, Plasma; e, EES; i, intracellular; t, body tissue); superscripts refer either to tumour (T), or body/systemic compartments (B). Model parameters for the drug delivery model are listed in Table 2. More detailed descriptions of the various terms in the equations can be found in a prior publication [16]).

TSL-DOX concentration in systemic plasma:

$$\frac{\mathrm{d}c_{p\_TSL}}{\mathrm{d}t} = -k_{e\_TSL}c_{p\_TSL} - R_{R37}c_{p\_TSL} \tag{4}$$

DOX concentration in systemic plasma:

$$\frac{\mathrm{d}c_p^B}{\mathrm{d}t} = \frac{\int_v (F_{pv}^T c_p^T v_p^T)\mathrm{d}V}{V_p^B} + c_{p\_TSL}R_{R37} - k_e c_p^B - k_p c_p^B + k_t c_t^B - c_p^B \frac{\int F_{pv}^T \mathrm{d}V}{V_p^B} v_p^T \tag{5}$$

DOX concentration in systemic tissue:

$$\frac{\mathrm{d}c_t^B}{\mathrm{d}t} = k_p c_p^B - k_t c_t^B \tag{6}$$

DOX concentration in tumour plasma:

$$\frac{\mathrm{d}c_p^T}{\mathrm{d}t} = -\frac{1}{v_p^T} PS\left(c_p^T - c_e^T\right) - F_{pv}^T c_p^T + F_{pv}^T c_p^B + c_{p\_TSL}R_R \tag{7}$$

DOX concentration in tumour EES:

$$\frac{\mathrm{d}c_p^T}{\mathrm{d}t} = \nabla \cdot (\mathrm{Diff} \cdot \nabla c_e^T) + \frac{1}{v_e^T} PS \cdot \left(c_p^T - c_e^T\right) - k_{3ci}\left(k_{1ci}c_e^T + \frac{k_{2ci}c_e^T}{k_{ici} + c_e^T} - c_i^T\right) \tag{8}$$

DOX concentration in cancer cells:

$$\frac{\mathrm{d}c_i^T}{\mathrm{d}t} = k_{3ci}\left(k_{1ci}c_e^T + \frac{k_{2ci}c_e^T}{K_{ici} + c_e^T} - c_i^T\right) \tag{9}$$

## Cell survival model

An exponential fit to the data from Kerr et al. [50] was used to calculate expected cell survival as a function of intracellular concentration. To compute overall cell survival, effect of heat and toxic effect of DOX were considered as independent. That means that the

estimated overall cell survival is the product of expected cell survival due to heat and expected cell survival due to DOX exposure.

### Heating regimen

TSL-DOX was allowed to circulate at 37°C for 15 min before heat was induced to emulate delay between administration and treatment in the clinics. Two different cases of tissue heating were modelled:

- Hyperthermia (HT), where tissue was heated to a target temperature $T_{set}$=43°C for 30 min.
- Hyperthermia followed by a short high temperature exposure (HT+), where tissue was heated with target temperature $T_{set}$=43°C, for 30 min, followed by a high temperature pulse with target temperature $T_{set}$=50°C for 20 s to cause vascular shut down, while limiting heat-induced cell death.
- In an additional simulation, the effect of HT duration on cell uptake was examined, where tissue temperature was kept constant at 43°C for an extended period of time (up to 5 h).

### Model for comparison to *in vivo* data

As preliminary validation of our modelling study, we compared the model to an *in vivo* experiment in a rabbit. This *in vivo* study employed a novel hyperthermia algorithm described in detail in the paper by Partanen et al. in this issue [51]. Briefly, the focal spot was moved along circular trajectories of 4 mm and 8 mm diameter to create a region of uniform temperatures. Average temperature along each trajectory was used in a binary feedback control algorithm, where sonication was initiated if temperature declined below 41°C, and sonication was stopped if temperature reached 42°C (implemented separately for 4 - and 8-mm trajectories). We implemented this algorithm in our heat transfer simulation to allow direct comparison to *in vivo* results, where HIFU heating profile used in the model was measured in phantoms as described earlier for both trajectories individually. This was a 2-D model in a plane orthogonal to the HIFU beam path (see Figure 2A, dashed line), i.e. not axi-symmetric as the models above. In addition, tissue baseline temperature in the model was reduced to 35°C to reproduce the conditions in the *in vivo* study.

### *In vivo* experiment

All animal-related procedures were approved and carried out under an animal use protocol approved by the USA's National Institutes of Health (NIH) Animal Care and Use Committee. Treatment set-up and animal handling/experimental procedures were the same as published earlier [29]. A lyso-lecithin containing TSL formulation with same release rate properties used in the simulations (ThermoDox(r), Celsion Corp., USA) was provided through a Collaborative Research and Development Agreement at a concentration of 1.8 mg doxorubicin/mL. Following anesthesia, a New Zealand White rabbit was infused with TSL at a dose of 5 mg DOX/kg body weight. Acoustic coupling was achieved by submerging the shaved thigh in a degassed water bath directly above the transducer. Body temperature (rectal) and breathing rate were monitored using standard MR-compatible devices. A

dedicated optical temperature probe (diameter 0.56 mm, Luxtron 3100, LumaSense Technologies, Santa Clara, CA, USA) was inserted in the thigh muscle near the location that was to be heated (outside of the HIFU beam path), and remained in the muscle throughout the treatment duration. The probe was used to acquire a baseline temperature for MR thermometry, prior to each sonication. Treatment was planned using a 3D coronal scan (3D turbo spin echo (TSE) sequence with repetition time (TR) 1600 ms, time to echo (TE) 30 ms, matrix of 640 × 640, field of view (FOV) 200 × 200 $mm^2$, slice thickness of 2 mm, stack of 80 slices, TSE factor 70, SENSE factor 2, bandwidth 585 Hz, coronal scan plane). MR thermometry as well as sonications were performed using a clinical MR-HIFU system (Sonalleve 1.5 T, Philips Medical Systems, Vantaa, Finland), as described in the phantom experiment above. Three 10-min sonications were performed sequentially at one location (i.e. total of 30 min HT) in the superficial thigh muscle of a New Zealand White rabbit ($n$ = 1), at an acoustic power of 25 W, using a sonication frequency of 1.2 MHz. All other characteristics of the system are explained in detail in the paper by Partanen et al. in this issue. A 5-min cool-down period between each sonication allowed temperature return to baseline. The target heating zone was the same size as in the computational model (8 mm diameter, ~20 mm length). Sonication was controlled based on average temperature along two circular trajectories of 4 mm and 8 mm in diameter in the coronal plane. Binary control was employed to maintain average trajectory temperature between 41–42°C for both trajectories, as in the computer model.

Following MR-HIFU + TSL-DOX therapy, distribution of DOX was evaluated with epifluorescent microscopy. Frozen tissue samples were sectioned with a thickness of 7 μm with a cryostat and stored at −80°C until further use. Slides were counterstained with TO-PRO®-3 (Invitrogen, Carlsbad, CA, USA) at 7–9 mM to identify nuclei, coverslipped (incubated 20–25 min), and then imaged. Imaging was performed with a 10 × objective (pixel size 2.58 μm) using an epi-fluorescent microscope (Zeiss, Axio Imager.M1, Thornwood, NY, USA) equipped with a monochrome CCD camera, motorised scanning stage, and mosaic stitching software (Axiovision, Zeiss). Two independent channels were obtained: Cy5 for nuclei (not shown in results) and a custom filter cube (ex: 480/40 nm, em: 600/60 nm, and dichroic: 505lp) corresponding to excitation and emission spectra of DOX.

## Results

Drug delivery by combination of HIFU and TSL was simulated for 30 min for two cases: 1) mild hyperthermia (HT); 2) mild hyperthermia followed by brief high temperature exposure (HT+).

### Heating and its effect on perfusion

The temperature distribution for the modelling study at the end of the 30-min heating for HT is shown on the left side of Figure 2A. The right image in Figure 2A shows perfusion relative to its starting value for HT. Hyperthermia caused a limited decrease in perfusion (it remained >75% of its initial value in the entire treatment cell). For HT and HT+ conditions, both temperature and perfusion changes are shown at the location of highest temperature (arrow in Figure 2A), in Figures 3A and 3C. Perfusion decreased linearly with time during

HT, and a nearly instantaneous termination of flow was observed once the temperature increased rapidly at the end of hyperthermia in the HT+ case (Figure 3C). Note that the model excluded any possible restoration of vascular function after flow cessation.

### Effects of heating/perfusion on drug delivery

In our simulation, following TSL administration, systemic and tumour plasma free drug concentrations increased to a maximum of 0.159 μg/g at $t = 6$ min due to slow DOX leakage of TSL at body temperature (this increase is not visible in the graphs in Figure 3B and 3D due to their scale). As a result, small amounts of DOX were taken up by EES and cells, resulting in slow increase in intracellular DOX concentration during the first 15 min (Figures 3B, 3D), before heat-triggered release. In the case of HT, DOX continuously accumulated in the central heated region for the entire heating duration (Figure 3B). DOX concentrations in plasma declined rapidly after heating was discontinued and TSL release stopped ($t = 45$ min). The low plasma concentrations result in back diffusion of DOX still present in EES into plasma, driving the decrease in the intracellular drug concentration after $t = 50$ min (Figure 3B). In contrast, the cessation of perfusion after heating in the HT+ scenario (Figure 3C) avoids any DOX back diffusion, resulting in prolonged DOX exposure of cells even after heating is discontinued (Figure 3D). Maximum cell concentration was 32.2 μg/g ($t = 80$ min) for HT+, and 22.8 μg/g ($t = 40$ min) for HT. Note that after cessation of perfusion in the HT+ case, the model does not allow for any transport to or from the plasma compartment; i.e. even though plasma concentrations are calculated in the model and presented in Figure 3D, they have no impact.

### Cellular damage induced by drug and heat

Thermally induced cell kill at the centre of the heating zone (i.e. location of maximum temperature of ~43°C, arrow in Figure 2B) resulted in survival fractions of 30% after HT and 15% after HT+. At the same location, DOX resulted in survival fractions of 33% after HT and 12% after HT+. Combining thermal and DOX-induced damage, overall survival was 3% after HT, and 1% after HT+. Outside the central region of temperatures exceeding 42°C (Figure 2A), DOX-induced cell damage dominates with negligible thermal damage (Figure 2B).

### Effect of hyperthermia exposure time on cellular drug uptake

In a separate model, the effect of hyperthermia duration on cellular DOX uptake was simulated (43°C hyperthermia for 5 h). A maximum intracellular DOX concentration of 47 μg/g was reached after approximately 2 h (Figure 4) and slowly decreased afterwards (data not shown). The maximum cell concentration occurred when equilibrium between active cell uptake and passive outward transport from cells takes place, and is mainly defined by TSL plasma half-life (i.e. with more stable TSL, even longer hyperthermia exposures would be beneficial).

### *In vivo* HIFU+TSL drug delivery and comparison to simulation

To observe drug delivery and compare *in vivo* and simulation results, MR-HIFU was used to provide HT treatment of a rabbit thigh muscle following an injection of TSL (Figure 5A).

The temperature profile was comparable between model and experiment (Figures 5B, 5E, 5F), with average temperature deviation of 0.54°C within the hyperthermic zone. *In vivo*, the heating resulted in a 41.7° ± 1.1°C (mean ± SD) temperature within the hyperthermic zone (T10 = 43.1°C, T90 = 40.3°C), with a mean thermal dose of 12.1 CEM43 (suggesting that no significant thermal damage was induced). The heating resulted in an enhanced DOX fluorescence signal in extracted tissue of the heated muscle region (microscopy image where maximum fluorescence was measured is presented in Figure 5C.). DOX distribution measured via fluorescence microscopy demonstrated ~6 times higher DOX fluorescence averaged over a 5 mm diameter concentric region around the target centre compared to regions ~15 mm distant from the target area (outside the field of view of Figure 5C). Simulated drug concentration profile qualitatively agreed in relative magnitude with the DOX fluorescence (Figure 5D). Note, however, that the simulation included a cell uptake model derived from lung cancer cells, as no mathematical model for muscle cells is available.

## Discussion

HIFU is a non-invasive technique that can be used to heat tissue to ablative temperatures, as well as to induce non-destructive hyperthermic temperatures (40–45°C). Via MR image guidance the focal zone can be positioned precisely in the target tissue. While HIFU ablation at temperatures above ~60°C allows rapid destruction of target tissue volumes, in many cases this approach is not sufficient or feasible. For example, specific anatomy, proximity of sensitive structures, or proximity of large vasculature may preclude complete tumour ablation. Further, many cancers (e.g. prostate and brain) represent diffuse disease that is not amenable to localised treatment and require a regional treatment approach. In these cases, the combination of HIFU with TSL can facilitate targeted drug delivery and consequently increase the anti-tumour effect [25, 52, 16, 26, 29]. However, there is a lack of data regarding optimal heating durations and the most advantageous temperature ranges. Computational models such as the one presented here can be used to quantify such parameters and help to carry out a preliminary selection for further experimental studies.

In the current study we combined a heat transfer model with a drug delivery model specific for a particular TSL-DOX formulation [29]. Experimental data derived from HIFU phantom experiments were used to extract the heating SAR profile of a clinical MR-HIFU system. This allowed us to simulate tissue heating, and calculate temperature and heat-induced perfusion changes for this HIFU system. The temperature and perfusion data were then used as input parameters in a drug delivery model.

Temperature-dependent liposomal drug release rate was based on prior *in vitro* studies [16, 17]. DOX transvascular transport, cellular uptake, as well as the expected cell survival of treated tumour cells were modelled based on prior experimental data [41, 50]. The combined model was then used to compare two different applications of heat: HT and HT+ in combination with administration of TSL-DOX.

### Hyperthermia

In the case of HT, mild hyperthermia was simulated for 30 min, which resulted in only minor reduction in perfusion (Figure 3A). Since temperatures above 44°C result in rapid loss of perfusion [36] and therefore reduced drug delivery, but temperatures above 40°C are necessary to trigger TSL drug release, tight temperature control is of great importance [53]. Liposomal release of DOX takes place within seconds at temperatures >40°C for the TSL formulation considered here [16]. Therefore, most of the release occurs during transit of TSL through the tumour microvasculature; this keeps concentration of bioavailable DOX (i.e. after release) in the tumour plasma elevated, with subsequent transport of DOX into EES and cell uptake (Figure 3B). When heating is discontinued, concentrations in tumour plasma and EES drop rapidly due to back diffusion of bioavailable DOX from EES into plasma, followed by removal due to perfusion. In response, intracellular DOX concentration starts to decrease soon after hyperthermia is discontinued, and EES concentration rapidly declines. Therefore, the peak intracellular concentration during HT was reached immediately after hyperthermia was discontinued (Figure 3B).

### Hyperthermia plus high temperature pulse

In this algorithm, an additional short high temperature pulse was applied following the 30 min hyperthermia period (Figure 3C). The aim was to stop perfusion (without heat-mediated cell kill, i.e. no thermal ablation), and Figure 3C confirms that in our model perfusion was reduced to almost zero. Hence no back diffusion of DOX from EES into plasma can take place (as was the case after discontinuation of hyperthermia for the HT case), and all DOX present within the EES is eventually taken up by cells; i.e. eliminating perfusion resulted in a depot of bioavailable DOX within the target region. As a result, peak intracellular concentration of DOX was increased by roughly a third compared to hyperthermia alone. Note that we did not consider any potential cytotoxic effects resulting from this elimination of perfusion, which may cause additional cell damage.

### Effect of hyperthermia exposure time on cell uptake

Duration of hyperthermia directly correlates with the amount of delivered drug, since cells continue to take up DOX as long as sufficient concentrations are present within the EES. Maximum intracellular concentration was obtained immediately following the end of heating in the case of HT (Figure 3B). To examine the effect of extended hyperthermia duration on cellular uptake, we assumed in a separate simulation constant hyperthermic temperatures for extended duration to find the maximum achievable cellular DOX concentration. The maximum intracellular concentration was reached after ~2 h of hyperthermia with 47 μg/g (Figure 4), and was primarily limited by the plasma half-life of 1.75 h for this type of TSL [7]. Therefore, longer heating durations than the 30 min considered above would lead to higher intracellular DOX concentrations and might be more effective for tumour treatment. In practice, 40 min of heat provides ~50% of the maximum concentration while 1 h provides ~75% of the maximum concentration. In addition, delivery could be enhanced by initiating heating as soon as possible after administration of drug or alternatively administering TSL-DOX during hyperthermia, again due to the relatively short plasma half-life of this TSL formulation (Figure 4).

### Cellular damage induced by drug and heat

Expected cell survival was calculated resulting from thermal exposure, as well as from DOX exposure. While the combination HT+DOX can produce synergistic cell kill [54, 55], no synergy effects were considered in our models. In the cases of HT and HT+, thermal damage of cells was generally negligible due to low thermal dose, except in the most central region where temperatures above 42°C were obtained (Figure 2A). The majority of cellular damage in the targeted tissue region was due to DOX uptake (Figure 2B). Complete cell death from DOX exposure, e.g. 99% cell kill would require intracellular concentrations of DOX of ~60 μg/g [50], which is considerably larger than achieved here. The bystander effect – which results in cell death due to destruction of neighbouring cancer/stroma cells – is not considered here and likely will provide additional cell kill, i.e. the achieved DOX concentrations are likely sufficient for complete destruction. Furthermore, survival will depend on cell type, i.e. quantitative data on cell uptake and survival for various cancer cell lines would improve accuracy of our models in predicting treatment effect for a particular cancer type.

### *In vivo* HIFU+TSL drug delivery and comparison to simulation

An *in vivo* study performed in rabbit thigh muscle, where HT was performed for a total of 30 min (Figure 5A), demonstrated ability of DOX delivery in a localised manner (Figure 5C). DOX fluorescence was ~6 times higher in the target region compared to muscle tissue regions distant from the hyperthermic region. The same hyperthermia algorithm used in *in vivo* study was implemented in the heat transfer model. As a result, the radial temperature profile closely matched between model and *in vivo* study, with ~0.5°C deviation on average (Figure 5B). Drug concentration profile from the simulation agreed well with fluorescence profile from the *in vivo* study (Figure 5D), though it should be noted that the exact location of the slide used to visualise DOX fluorescence relative to the targeted region is not exactly known. The presented comparison to preliminary *in vivo* results thus suggests feasibility of the modelling approach presented, in both predicting tissue temperature profile during HIFU-mediated hyperthermia as well as in estimating the amount of delivered drug.

## Conclusions

We present computer simulations to predict the amount of delivered drug for different heat exposures, and estimate achieved cell kill by both heat and drug. Our models suggest a direct correlation between hyperthermia duration and drug uptake by cancer cells. Maximum concentration of drug was achieved after 2 h of hyperthermia. Cell uptake may be also enhanced by heat-induced vascular shutdown following hyperthermia, which facilitates a drug depot effect. Modelling results agree with preliminary *in vivo* results in a rabbit animal model with regard to both temperature and drug concentration. After further validation, computer models may thus allow quantitative comparison of different heating algorithms, and facilitate treatment planning for this targeted drug delivery paradigm.

## Acknowledgments

This work was supported by US National Institutes of Health (NIH) grants R01CA118990, R21CA135519 to DH, by the NIH Center for Interventional Oncology and the NIH Intramural Research Program, and by a cooperative

research agreement between NIH and Philips. NIH and Celsion Corporation have a Cooperative Research and Development Agreement. Part of the work was conducted in a facility constructed with support from the NIH, grant number C06 RR018823 from the Extramural Research Facilities Program of the National Center for Research Resources. A.P. is employed by Philips Healthcare.

## References

1. Allen TM, Cullis PR. Drug delivery systems: Entering the mainstream. Science. 2004; 303:1818–1822. [PubMed: 15031496]
2. Matsumura Y, Maeda H. A new concept for macromolecular therapeutics in cancer-chemotherapy – Mechanism of tumoritropic accumulation of proteins and the antitumor agent SMANCS. Cancer Res. 1986; 46:6387–6392. [PubMed: 2946403]
3. Poon, RT, Ng, KK, Yuen, J, Hahne, W, Prabhakar, R, Eugeni, M. , et al. A Phase I Dose Escalation Tolerability Study of ThermoDox™ (Thermally Sensitive Liposomal Doxorubicin) in Combination With Radiofrequency Ablation (RFA) of Primary and Metastatic Tumors of the Liver. Columbia, MD: Celsion Corporation;
4. Celsion. A phase III, randomized, double-blinded, dummy-controlled study of the efficacy and safety of ThermoDox® (thermally sensitive liposomal doxorubicin) in combination with radiofrequency ablation (RFA) compared to RFA-alone in the treatment of non-resectable hepatocellular carcinoma. Clinical trial.
5. National Cancer Institute. A phase I dose escalation study of heat activated liposome delivery of doxorubicin and radio-frequency ablation of primary and metastatic tumors of the liver. Clinical trial National Institutes of Health.
6. Duke University Cancer Institute and National Cancer Institute. A phase I, dose escalation and pharmacokinetics study of temperature sensitive liposome encapsulated doxorubicin (ThermoDox™) and hyperthermia in patients with local-regionally recurrent breast cancer. Clinical trial National Institutes of Health.
7. Poon RT, Borys N. Lyso-thermosensitive liposomal doxorubicin: A novel approach to enhance efficacy of thermal ablation of liver cancer. Expert Opin Pharmacother. 2009; 10:333–3343. [PubMed: 19236203]
8. Yatvin MB, Weinstein JN, Dennis WH, Blumenthal R. Design of liposomes for enhanced local release of drugs by hyperthermia. Science. 1978; 202:1290–1293. [PubMed: 364652]
9. Merlin JL. Encapsulation of doxorubicin in thermosensitive small unilamellar vesicle liposomes. Eur J Cancer. 1991; 27:1026–1030. [PubMed: 1832888]
10. Gaber MH, Hong K, Huang SK, Papahadjopoulos D. Thermosensitive sterically stabilized liposomes: Formulation and *in vitro* studies on mechanism of doxorubicin release by bovine serum and human plasma. Pharm Res. 1995; 12:1407–1416. [PubMed: 8584472]
11. Kong G, Anyarambhatla G, Petros WP, Braun RD, Colvin OM, Needham D, et al. Efficacy of liposomes and hyperthermia in a human tumor xenograft model: Importance of triggered drug release. Cancer Res. 2000; 60:6950–6957. [PubMed: 11156395]
12. Needham D, Dewhirst MW. The development and testing of a new temperature-sensitive drug delivery system for the treatment of solid tumors. Adv Drug Deliv Rev. 2001; 53:285–305. [PubMed: 11744173]
13. Li L, ten Hagen TL, Schipper D, Wijnberg TM, van Rhoon GC, Eggermont AM, et al. Triggered content release from optimized stealth thermosensitive liposomes using mild hyperthermia. J Control Release. 2010; 143:274–279. [PubMed: 20074595]
14. Kong G, Braun RD, Dewhirst MW. Characterization of the effect of hyperthermia on nanoparticle extravasation from tumor vasculature. Cancer Res. 2001; 61:3027–3032. [PubMed: 11306483]
15. Hossann M, Wiggenhorn M, Schwerdt A, Wachholz K, Teichert N, Eibl H, et al. *In vitro* stability and content release properties of phosphatidylglyceroglycerol containing thermo-sensitive liposomes. Biochim Biophys Acta. 2007; 1768:2491–2499. [PubMed: 17618599]
16. Gasselhuber A, Dreher MR, Negussie A, Wood BJ, Rattay F, Haemmerich D. Mathematical spatio-temporal model of drug delivery from low temperature sensitive liposomes during radiofrequency tumour ablation. Int J Hyperthermia. 2010; 26:499–513. [PubMed: 20377363]

17. Negussie AH, Yarmolenko PS, Partanen A, Ranjan A, Jacobs G, Woods D, et al. Formulation and characterisation of magnetic resonance imageable thermally sensitive liposomes for use with magnetic resonance-guided high intensity focused ultrasound. Int J Hyperthermia. 2011; 27:140–155. [PubMed: 21314334]
18. Rumboldt Z, Al-Okaili R, Deveikis JP. Perfusion CT for head and neck tumors: Pilot study. Am J Neuroradiol. 2005; 26:1178–1185. [PubMed: 15891181]
19. Abdullah SS, Pialat JB, Wiart M, Duboeuf F, Mabrut JY, Bancel B, et al. Characterization of hepatocellular carcinoma and colorectal liver metastasis by means of perfusion MRI. J Magn Reson Imaging. 2008; 28:390–395. [PubMed: 18666145]
20. Ludemann L, Prochnow D, Rohlfing T, Franiel T, Warmuth C, Taupitz M, et al. Simultaneous quantification of perfusion and permeability in the prostate using dynamic contrast-enhanced magnetic resonance imaging with an inversion-prepared dual-contrast sequence. Ann Biomed Eng. 2009; 37:749–762. [PubMed: 19169821]
21. Hokland SL, Pedersen M, Salomir R, Quesson B, Stodkilde-Jorgensen H, Moonen CT. MRI-guided focused ultrasound: Methodology and applications. IEEE Trans Med Imaging. 2006; 25:723–731. [PubMed: 16768237]
22. ter Haar G, Coussios C. High intensity focused ultrasound: Physical principles and devices. Int J Hyperthermia. 2007; 23:89–104. [PubMed: 17578335]
23. Staruch R, Chopra R, Hynynen K. MRI-controlled ultrasound thermal therapy. IEEE Pulse. 2011; 2:39–47.
24. Tempany CM, McDannold NJ, Hynynen K, Jolesz FA. Focused ultrasound surgery in oncology: Overview and principles. Radiology. 2011; 259:39–56. [PubMed: 21436096]
25. Dromi S, Frenkel V, Luk A, Traughber B, Angstadt M, Bur M, et al. Pulsed-high intensity focused ultrasound and low temperature-sensitive liposomes for enhanced targeted drug delivery and antitumor effect. Clin Cancer Res. 2007; 13:2722–2727. [PubMed: 17473205]
26. Staruch R, Chopra R, Hynynen K. Localised drug release using MRI-controlled focused ultrasound hyperthermia. Int J Hyperthermia. 2010; 27:156–171. [PubMed: 21158487]
27. de Smet M, Heijman E, Langereis S, Hijnen NM, Grull H. Magnetic resonance imaging of high intensity focused ultrasound mediated drug delivery from temperature-sensitive liposomes: An *in vivo* proof-of-concept study. J Control Release. 2011; 150:102–110. [PubMed: 21059375]
28. Gasselhuber A, Appanaboyina S, Dreher MR, Partanen A, Wood BJ, Rattay F. Computational modeling of high-intensity focused ultrasound mediated drug delivery. Proc SPIE. 2011; 7901:7910F.
29. Ranjan A, Jacobs GC, Woods DL, Negussie AH, Partanen A, Yarmolenko PS, et al. Image-guided drug delivery with magnetic resonance guided high intensity focused ultrasound and temperature sensitive liposomes in a rabbit VX2 tumor model. J Control Release. 2012; 158:487–494. [PubMed: 22210162]
30. El-Kareh AW, Secomb TW. Theoretical models for drug delivery to solid tumors. Crit Rev Biomed Eng. 1997; 25:503–571. [PubMed: 9719859]
31. El-Kareh AW, Secomb TW. A mathematical model for comparison of bolus injection, continuous infusion, and liposomal delivery of doxorubicin to tumor cells. Neoplasia. 2000; 2:325–338. [PubMed: 11005567]
32. Zhang A, Mi X, Yang G, Xu LX. Numerical study of thermally targeted liposomal drug delivery in tumor. J Heat Transfer. 2009; 131:043209–0432010.
33. Pennes HH. Analysis of tissue and arterial blood temperatures in the resting human forearm. J Appl Physiol. 1948; 1:93–122. [PubMed: 18887578]
34. Partanen A, Mougenot C, Vaara T. Feasibility of agar-silica phantoms in quality assurance of MRgHIFU. AIP Conference Proceedings. 2009; 1113:296–300.
35. Ishihara Y, Calderon A, Watanabe H, Okamoto K, Suzuki Y, Kuroda K. A precise and fast temperature mapping using water proton chemical shift. Magn Reson Med. 1995; 34:814–823. [PubMed: 8598808]
36. Brown SL, Hunt JW, Hill RP. Differential thermal sensitivity of tumour and normal tissue microvascular response during hyperthermia. Int J Hyperthermia. 1992; 8:501–514. [PubMed: 1402130]

37. Breen MS, Breen M, Butts K, Chen L, Saidel GM, Wilson DL. MRI-guided thermal ablation therapy: Model and parameter estimates to predict cell death from mr thermometry images. Ann Biomed Eng. 2007; 35:1391–1403. [PubMed: 17436111]
38. Duck, FA. Chapter 2: Thermal properties of tissue Physical properties of tissue. London: Academic Press; 1990. 167–223.
39. Van Beers BE, Leconte I, Materne R, Smith AM, Jamart J, Horsmans Y. Hepatic perfusion parameters in chronic liver disease: Dynamic CT measurements correlated with disease severity. Am J Roentgenol. 2001; 176:667–673. [PubMed: 11222202]
40. Gustafson DL, Rastatter JC, Colombo T, Long ME. Doxorubicin pharmacokinetics: Macromolecule binding, metabolism, and excretion in the context of a physiologic model. J Pharm Sci. 2002; 91:1488–1501. [PubMed: 12115848]
41. El-Kareh AW, Secomb TW. Two-mechanism peak concentration model for cellular pharmacodynamics of doxorubicin. Neoplasia. 2005; 7:705–713. [PubMed: 16026650]
42. Tofts PS, Brix G, Buckley DL, Evelhoch JL, Henderson E, Knopp MV, et al. Estimating kinetic parameters from dynamic contrast-enhanced t(1)-weighted MRI of a diffusable tracer: Standardized quantities and symbols. J Magn Reson Imaging. 1999; 10:223–232. [PubMed: 10508281]
43. Brizel DM, Klitzman B, Cook JM, Edwards J, Rosner G, Dewhirst MW. A comparison of tumor and normal tissue microvascular hematocrits and red cell fluxes in a rat window chamber model. Int J Radiat Oncol Biol Phys. 1993; 25:269–276. [PubMed: 8420874]
44. Sparano JA, Speyer J, Gradishar WJ, Liebes L, Sridhara R, Mendoza S, et al. Phase I trial of escalating doses of paclitaxel plus doxorubicin and dexrazoxane in patients with advanced breast cancer. J Clin Oncol. 1999; 17:880–886. [PubMed: 10071279]
45. Jackson TL. Intracellular accumulation and mechanism of action of doxorubicin in a spatiotemporal tumor model. J Theor Biol. 2003; 220:201–213. [PubMed: 12468292]
46. Brown RP, Delp MD, Lindstedt SL, Rhomberg LR, Beliles RP. Physiological parameter values for physiologically based pharmacokinetic models. Toxicol Ind Health. 1997; 13:407–484. [PubMed: 9249929]
47. Yuan F, Leunig M, Berk DA, Jain RK. Microvascular permeability of albumin, vascular surface area, and vascular volume measured in human adenocarcinoma LS174T using dorsal chamber in SCID mice. Microvasc Res. 1993; 45:269–289. [PubMed: 8321142]
48. Jain RK. Transport of molecules in the tumor interstitium: A review. Cancer Res. 1987; 47:3039–3051. [PubMed: 3555767]
49. Qian F, Stowe N, Liu EH, Saidel GM, Gao J. Quantification of *in vivo* doxorubicin transport from PLGA millirods in thermoablated rat livers. J Control Release. 2003; 91:157–166. [PubMed: 12932647]
50. Kerr DJ, Kerr AM, Freshney RI, Kaye SB. Comparative intracellular uptake of adriamycin and 4′-deoxydoxorubicin by non-small cell lung tumor cells in culture and its relationship to cell survival. Biochem Pharmacol. 1986; 35:2817–2823. [PubMed: 3741470]
51. Partanen A, Yarmolenko PS, Viitala A, Appanaboyina S, Haemmmerich D, Ranjan A, et al. Mild hyperthermia with magnetic resonance guided high intensity focused ultrasound for applications in drug delivery. Int J Hyperthermia. 2012
52. Patel PR, Luk A, Durrani A, Dromi S, Cuesta J, Angstadt M, et al. *In vitro* and *in vivo* evaluations of increased effective beam width for heat deposition using a split focus high intensity ultrasound (HIFU) transducer. Int J Hyperthermia. 2008; 24:537–549. [PubMed: 18608578]
53. Mougenot C, Quesson B, de Senneville BD, de Oliveira PL, Sprinkhuizen S, Palussiere J, et al. Three-dimensional spatial and temporal temperature control with MR thermometry-guided focused ultrasound (MRGHIFU). Magn Reson Med. 2009; 61:603–614. [PubMed: 19097249]
54. Kawai H, Minamiya Y, Kitamura M, Matsuzaki I, Hashimoto M, Suzuki H, Abo S. Direct measurement of doxorubicin concentration in the intact, living single cancer cell during hyperthermia. Cancer. 1997; 79:214–219. [PubMed: 9010093]
55. Goldberg SN, Saldinger PF, Gazelle GS, Huertas JC, Stuart KE, Jacobs T, et al. Percutaneous tumor ablation: Increased necrosis with combined radio-frequency ablation and intratumoral

doxorubicin injection in a rat breast tumor model. Radiology. 2001; 220:420–427. [PubMed: 11477246]

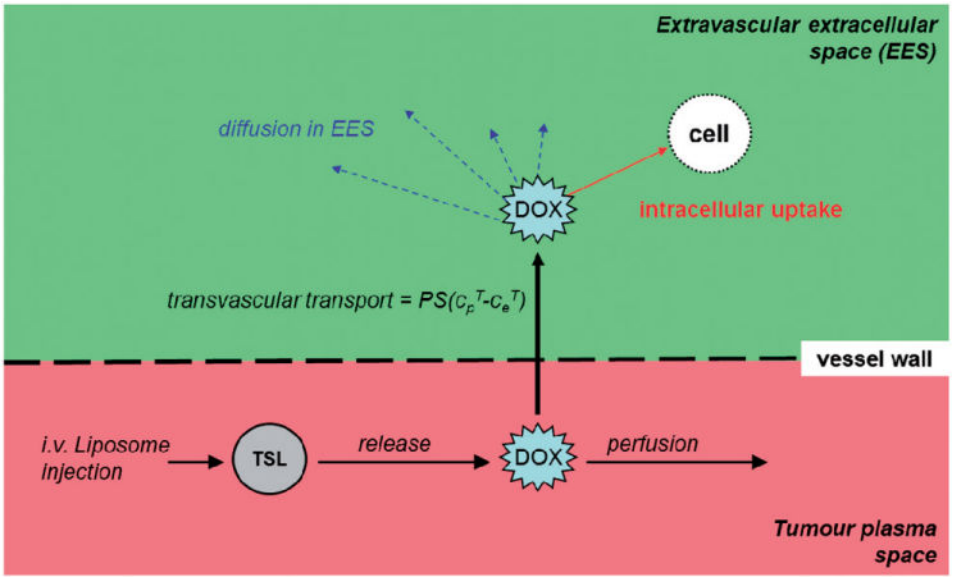


**Figure 1.**

Drug delivery model overview. After TSL are exposed to hyperthermia, drug is released at the target site at a rate depending on local temperature. Released drug can cross the vessel wall into the EES, where drug diffuses and intracellular uptake takes place. Drug not taken up by tissue is removed from the tumour plasma by blood perfusion (Figure reproduced from Gasselhuber et al. [16]).

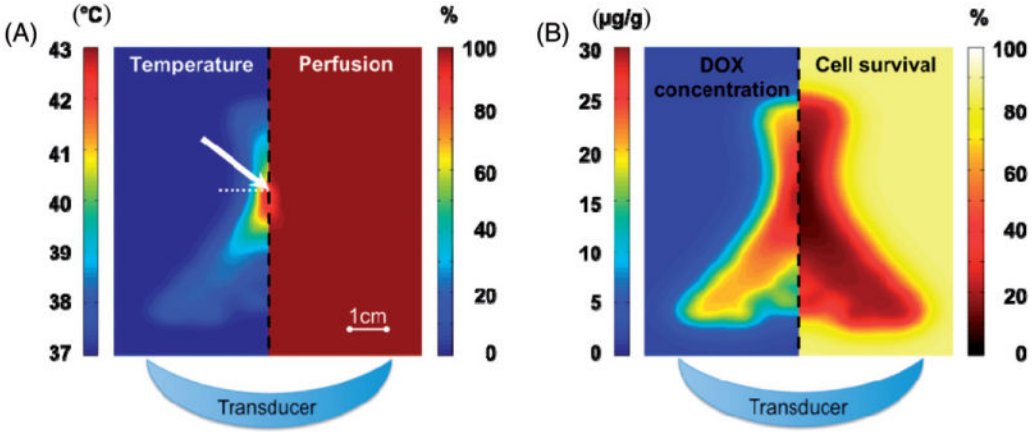


**Figure 2.**

Computer model results in plane parallel to the HIFU beam path (transducer position illustrated at bottom) shown for hyperthermia (HT) regimen (target temperature 43°C). (A) Temperature map at the end of 30 min heating (left), corresponding perfusion map (right). (B) Intracellular DOX concentration 35 min after initiation of HIFU (left), and resulting cell survival due to cellular DOX uptake (right). White arrow in (A) indicates location corresponding to Figure 3 plots and the white dashed line indicates the plane parallel to transducer, corresponding to results in Figure 5.

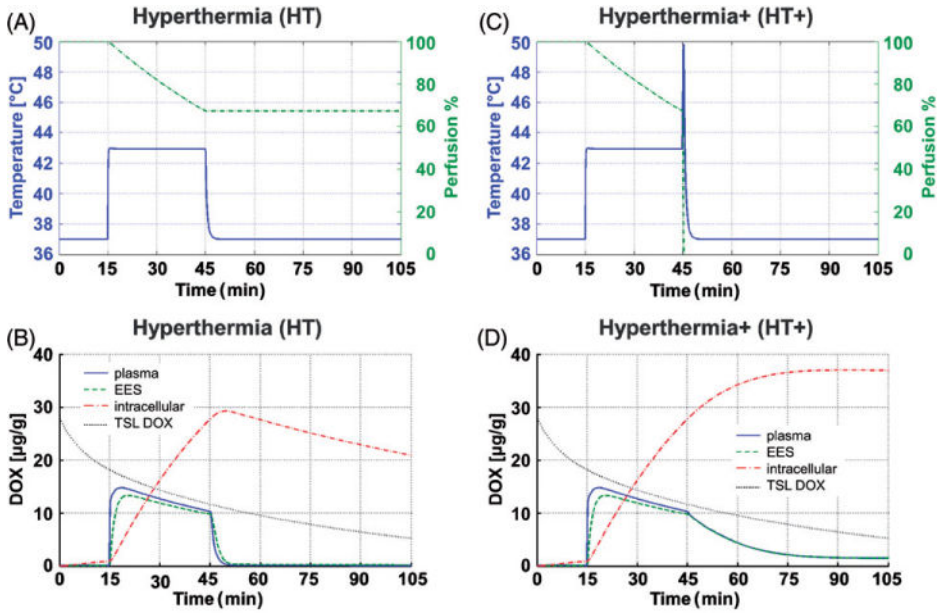


**Figure 3.**

(A) Temperature and perfusion time course for HT case, and (B) corresponding concentrations of TSL-DOX, and bioavailable DOX in plasma, EES and cells. (C) Temperature and perfusion time course for the HT+ case, and (D) corresponding DOX concentrations in tumour compartments. All data are shown at the location of highest temperature (white arrow in Figure 2A).

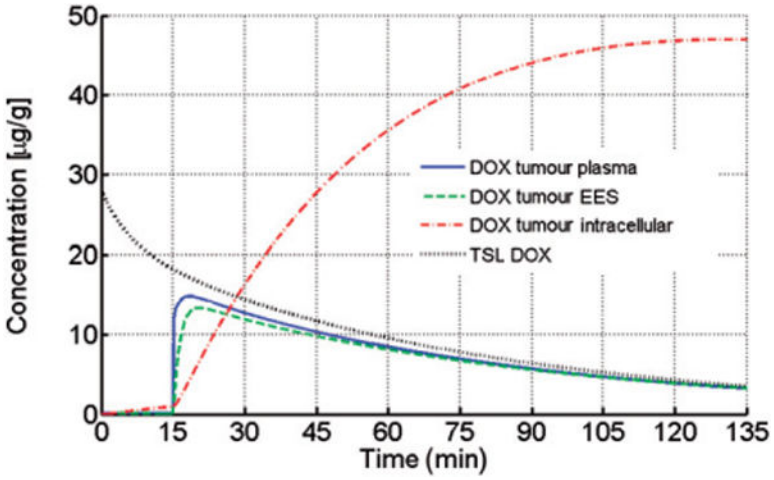


**Figure 4.**

Effect of hyperthermia exposure duration on drug uptake, assuming a constant temperature of 43°C after $t = 15$ min. TSL-DOX concentration decreases due to limited TSL stability in plasma. Maximum intracellular DOX concentration was reached after ~2 h of hyperthermia, and limited by TSL-DOX plasma half-life.

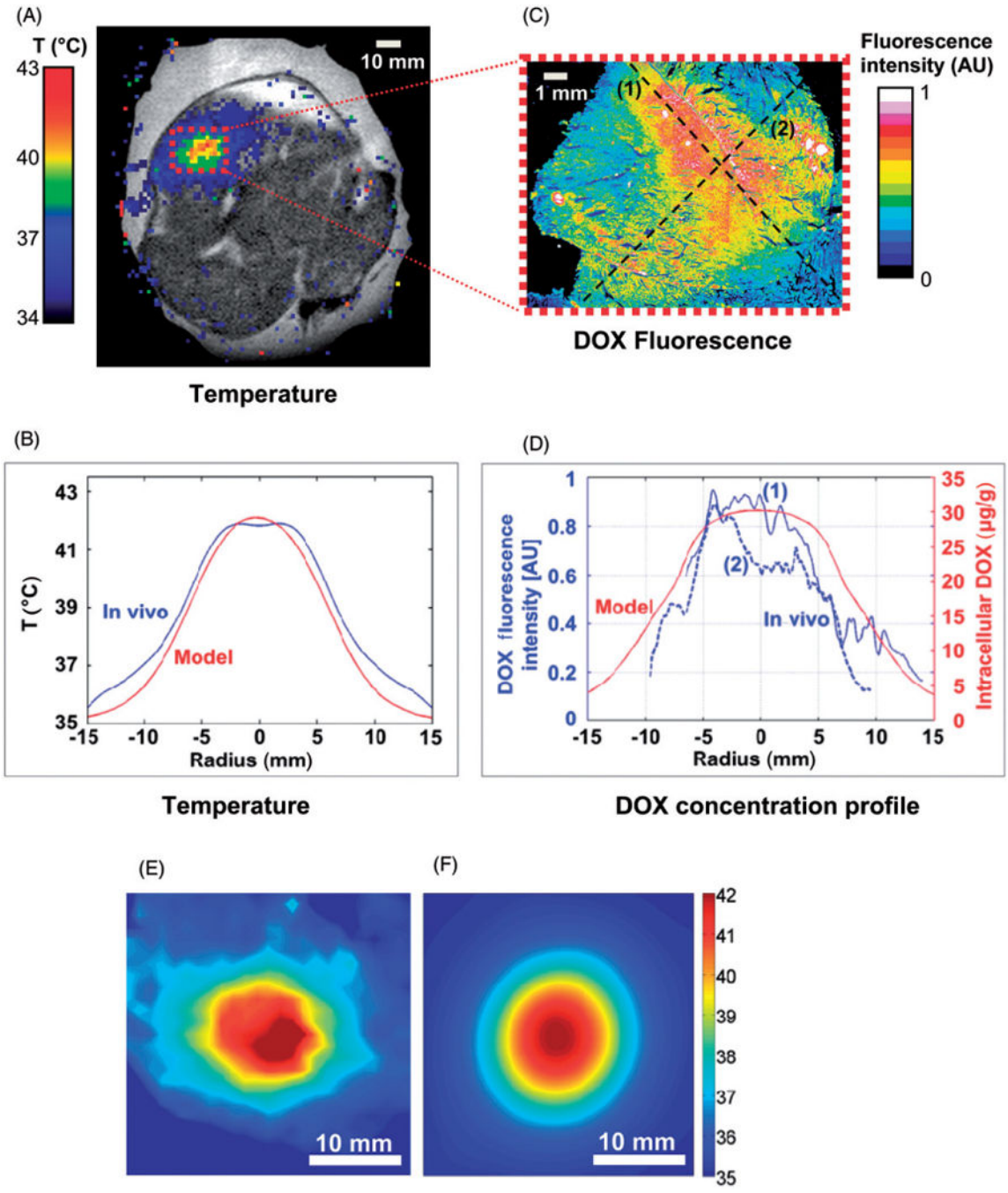


**Figure 5.**

(A) Temperature map during HT measured via MR Thermometry, overlaid on pre-procedural proton density-weighted coronal image of rabbit thigh muscle. (B) Radial temperature profile (time-averaged over HT duration) from *in vivo* study (blue), compared to model (red). Profile location in model was chosen such that it traversed maximum temperature point (see Figure 2A, white dashed line). Temperature deviation between simulation and *in vivo* study was 0.54°C (mean over 15 mm radius). (C) DOX distribution measured via fluorescence microscopy in extracted tissue sample. (D) DOX fluorescence

profile (blue) in two orthogonal directions (dashed lines marked (1) and (2) in (C), compared to DOX concentration profile from computer model (red). Mean temperature map (time-averaged over HT duration) is shown for the *in vivo* experiment (E), and the modelling study (F). All results are shown in the plane perpendicular to the HIFU beam path (see dashed line in Figure 2A).

**Table 1**

Parameters of the HIFU heat transfer model.

| Symbol | Description | Value | Source |
|---|---|---|---|
| $\rho$ | Mass density of tissue | 1060 kg $m^{-3}$ | [38] |
| $c$ | Specific heat of tissue | 3600 J $kg^{-1}K^{-1}$ | [38] |
| $k$ | Thermal conductivity of tissue | 0.6 W $m^{-1}K^{-1}$ | [38] |
| $c_{bl}$ | Specific heat of blood | 3800 J $kg^{-1}K^{-1}$ | [38] |
| $w_{bl}$ | Blood perfusion rate | 0.018 $s^{-1}$ | [39] |
| $T_{bl}$ | Arterial blood temperature | 37°C | NA |
| $k_p$ | Controller parameter (proportional term) | 0.2 | NA |
| $k_i$ | Controller parameter (integral term) | 0.01 | NA |
| $A$ | Frequency factor for perfusion decrease | 8.056e160 $s^{-1}$ | Fitted to prior data [36] |
| $\Delta E$ | Activation energy for perfusion decrease | 9.960e5 J $mole^{-1}$ | Fitted to prior data [36] |
| $A$ | Frequency factor for cell survival | 2.95e80 $s^{-1}$ | [37] |
| $\Delta E$ | Activation energy for cell survival | 5.064e5 J $mole^{-1}$ | [37] |
| $R$ | Universal gas constant | 8.314 J $mole^{-1}$ K | NA |

**Table 2**

Parameters for the drug delivery model.

| Symbol | Description | Value | Source |
|---|---|---|---|
| $Hct$ | Haematocrit | 0.45 | [42] |
| $Hct_{tumour}$ | Haematocrit for tumour microvasculature | 0.19 | [43] |
| $k_p$ | Transfer constant from systemic plasma to tissue | 1.6e–3 $s^{-1}$ | Calculated with parameters from [44] |
| $k_e$ | Transfer constant for clearance | 1.1e–3 $s^{-1}$ | Calculated with parameters from [44] |
| $k_t$ | Transfer constant from tissue to systemic plasma | 4.6809e–5 $s^{-1}$ | Calculated with parameters from [44] |
| $k_{e\_TSL}$ | Rate constant of TSL clearance | 2.228e–4 $s^{-1}$ | Fitted to data from [7] |
| $k_{1ci}$ | Parameter for intracellular uptake | 2.2572 | [41] |
| $k_{2ci}$ | Parameter for intracellular uptake | 0.0452 $kg/m^3$ | [41] |
| $k_{3ci}$ | Parameter for intracellular uptake | 2.8056e–4 $s^{-1}$ | [41] |
| $K_{ici}$ | Parameter for intracellular uptake | 5.2875e–4 $kg/m^3$ | [41] |
| $PS$ | Permeability surface area product for DOX | 7e–3 $s^{-1}$ | [45] |
| $V_B^B$ | Total blood volume in body | 5.53 L | Calculated with: blood = 7.9% of body weight [46] |
| $V_p^B$ | Volume of systemic plasma | 3.04 L | $V_B^B(1 - Hct)$ |
| $V_{tissue}$ | Volume for body tissue (organs, etc.) | 64.47 L | Calculated with: blood = 7.9% of body weight [46] |
| $V_v^T$ | Volume fraction of tumour vascular space | 0.092 | [47] |
| $V_p^T$ | Volume fraction of tumour plasma space | 0.07452 | $V_v^T(1 - Hct_{tumour})$ |
| $V_e^T$ | Volume fraction of tumour EES | 0.454 | [48] |
| $V_i^T$ | Volume fraction of tumour intracellular space | 0.454 | $(1 - v_V^T - v_e^T)$ |
| $R_R$ | Release rate of DOX from TSL | variable ($s^{-1}$) | [16] |
| $R_{R37}$ | Release rate of DOX from TSL at 37°C | variable ($s^{-1}$) | [16] |
| $rf$ | Release fraction of DOX from TSL | variable | biexponential fit |
| $F_{pv}^T$ | Plasma flow in tumour plasma space<br>Note: $F_{pv}$ = plasma flow/plasma volume | variable ($s^{-1}$) | Calculated with heat transfer model |
| $T$ | Temperature | variable (°C) | Calculated with heat transfer model |
| $Diff$ | Diffusion coefficient for ablated tissue | 1.1e–7 $cm^2/s$ | [49] |
| | Diffusion coefficient for non-ablated tissue | 6.7e–7 $cm^2/s$ | |